rable temperatures, the crystallization of babingtonite requires more hydrous conditions, lower CO_2, and slightly higher O_2 fugacities in the fluid phase than ilvaite. Since similar temperatures, CO_2 pressures, and oxygen fugacities induced within skarn deposits exist on Venus, ilvaite and perhaps babingtonite could have also formed on the surface of this planet by the interaction of the venusian atmosphere with extruded basaltic rocks. One factor that might mitigate against the formation of these calcic Fe^{2+}-Fe^{3+} silicates on Venus, however, are the high abundances of Mg and Al measured during the Venera 13/14 [32] and Vega 2 [33] missions. The Mg^{2+} and Al^{3+} cations are not accepted into the crystal structures of ilvaite and babingtonite.

Discussion: Although magnetite is generally regarded to be the predominant ferric-bearing mineral on Venus, other mixed-valence Fe^{2+}-Fe^{3+} minerals known to exist on the surface of Earth could be stable in the venusian atmosphere. Thus, in addition to laihunite (which is probably metastable) and ilvaite and babingtonite (both of which may be found in rocks depleted of Mg and Al), oxy-amphiboles and oxy-micas may also be major constituents of the venusian surface. The opacities and high electrical conductivities of such mixed-valence Fe^{2+}-Fe^{3+} silicate minerals, the properties of which resemble magnetite [34], may also contribute to high radar-reflectivity regions in the highlands of Venus [35].

References: [1] Volkov V. P. et al. (1986) *Adv. Phys. Geochem.*, *6*, 136–190. [2] Gooding J. L. (1986) in *The Solar System Observations and Interpretations* (M. G. Kivelson, ed.), 208–299, Prentice-Hall. [3] Fegley B. Jr. et al. (1992) *Proc. LPSC, Vol. 22*, 3–19. [4] Florensky C. P. et al. (1983) *LPSC XIV*, 203–204. [5] Pieters C. M. et al. (1986) *Science, 234*, 1379–1383. [6] Barsukov V. L. et al. (1982) *Proc. LPSC 13th*, in *JGR, 87*, A3–A9. [7] Nozette S. and Lewis J. S. (1982) *Science, 216*, 181–183. [8] Bartels K. S. and Burns R. G. (1986) *Eos, 44*, 1270. [9] Bartels K. S. and Burns R. G. (1989) *Intl. Geol. Congr., 28*, 9293. [10] Bartels K. S. and Burns R. G. (1989) *LPSC XX*, 44–45. [11] Straub D. W. et al. (1991) *JGR, 96*, 18819–18830. [12] Straub D. W. and Burns R. G. (1992) *LPSC XXIII*, 1375–1376. [13] Zhang R. et al. (1981) *Tscher. Mineral. Petrog. Mitt., 28*, 167–187. [14] Schaefer M. W. (1983) *Nature, 303*, 325–327. [15] Schaefer M. W. (1985) *Am. Mineral., 70*, 729–736. [16] Kondoh S. et al. (1985) *Am. Mineral., 70*, 737–746. [17] Banfield J. F. et al. (1990) *Contrib. Mineral. Petrol., 106*, 110–123. [18] Iishi K. et al. (1989) *Neues Jahrb. Mineral. Mh., H6*, 245–254. [19] Iishi K. et al. (1989) *Neues Jahrb. Mineral. Mh., H8*, 345–356. [20] Kitamura M. et al. (1984) *Am. Mineral., 69*, 154–160. [21] Shen B. et al. (1986) *Am. Mineral., 71*, 1455–1460. [22] Wang S.-Y. (1980) *Geochimica (Chinese), 3*, 31–42. [23] Khodakovsky I. L. et al. (1979) *Icarus, 39*, 352–363. [24] Barnes V. E. (1930) *Am. Mineral., 15*, 393–417. [25] Phillips M. W. et al. (1988) *Am. Mineral., 73*, 500–506. [26] Phillips M. W. et al. (1989) *Am. Mineral., 74*, 764–773. [27] Popp R. K. et al. (1990) *Am. Mineral., 75*, 163–169. [28] Burt D. M. (1971) *Annu. Rept. Geophys. Lab. Yearb., 70*, 189–197. [29] Burt D. M. (1971) *Soc. Mining Geol. Japan, Spec. Issue 3*, 375–380. [30] Gustafson H. J. (1967) *J. Petrol., 15*, 455–496. [31] Gole M. J. (1981) *Can. Mineral., 19*, 269–277. [32] Surkov Y. A. et al. (1984) *Proc. LPSC 14th*, in *JGR, 89*, B393–B402. [33] Surkov Y. A. et al. (1986) *Proc. LPSC 16th*, in *JGR, 91*, E215–E218. [34] Burns R. G. (1991) in *Mixed-Valence Systems: Applications in Chemistry, Physics and Biology* (K. Prassides, ed.), 175–200, NATO ASI-C Ser., Math. Phys. Sci., 343, Plenum. [35] Research supported by NASA grant number NAGW-2049.

THERMAL BUOYANCY ON VENUS: PRELIMINARY RESULTS OF FINITE ELEMENT MODELING.

J. D. Burt and J. W. Head, Department of Geological Sciences, Brown University, Providence RI 02912, USA.

Introduction: Enhanced surface temperatures and a thinner lithosphere on Venus relative to Earth have been cited as leading to increased lithospheric buoyancy. This would limit [1] or prevent [2] subduction on Venus and favor the construction of thickened crust through underthrusting. Underthrusting may contribute to the formation of a number of features on Venus. For example, Freyja Montes, a linear mountain belt in the northern hemisphere of Venus, has been interpreted to be an orogenic belt [3] and a zone of convergence and underthrusting of the north polar plains beneath Ishtar Terra, with consequent crustal thickening [4]. Such mountain belts lie adjacent to regions of tessera and contain evidence of volcanic activity. Tessera is also considered to consist of thickened crust [5] and crustal underthrusting is one possible mode for its formation [4]. Models for the formation of the mountain belts and associated features must then explain compressional deformation and crustal thickening, as well as melt production.

In order to evaluate the conditions distinguishing between underthrusting and subduction, we have modeled the thermal and buoyancy consequences of the subduction end member. This study considers the fate of a slab from the time it starts to subduct, but bypasses the question of subduction initiation. Thermal changes in slabs subducting into a mantle having a range of initial geotherms are used to predict density changes and thus their overall buoyancy. Finite element modeling is then applied in a first approximation of the assessment of the relative rates of subduction as compared to the buoyant rise of the slab through a viscous mantle.

Subduction Model: In the model, slabs, having a thickness set by 90% of the basalt solidus, subduct at a 45° angle into the mantle. The initial geotherms match surface thermal gradients of 10°C/km, 15°C/km, and 25°C/km [6]. Slabs heat via conduction, crustal radioactivity, phase changes, and adiabatic compression. Phase changes involving the conversion of basalt to eclogite at depths of 60 to 160 km and then enstatite to forsterite plus stishovite between 260 and 360 km generate 0.13×10^{-5} ergs/cm^3 s and 0.36×10^{-5} ergs/cm^3 s respectively [7]. The slab radiogenic heat production is 2.63×10^{-7} ergs/g s [8]. Adiabatic compression adds 0.5°C per kilometer of depth. Convergence rates ranged from 5 mm/yr to 100 mm/yr.

The thermal evolution of the slab is followed using a finite difference technique [7,9]. The model region measures 800 km horizontally by 400 km deep. Processing ends when the slab tips reach a 300-km depth, implying time intervals of 10 m.y. to 100 m.y. Slab density changes derive from the thermal results through calculation of the thermal expansion ($a_v = 3 \times 10^{-5}$/°K [8]) and the effects of pressure ($b = 1 \times 10^{-3}$/kbar [8]) on initial densities set for zero pressure and temperature. The assumed initial density structure includes a 10-km or 25-km basaltic crust (density = 3.0 g/cm^3), a corresponding 25-km or 65-km-thick depleted mantle zone (density = 3.295 g/cm^3), and an underlying undepleted mantle (density = 3.36 g/cm^3). Density changes due to the phase transitions are also included. Results take the form of density distributions within the model region.

Finite element modeling is then employed to gauge the rate at which a slab having the density structure derived above will move through a viscous mantle. Buoyancy body forces are applied to a slab having a viscosity of 10^{21} Pa s surrounded by a mantle with a

viscosity of 10^{19} Pa s. Zero stress boundary conditions are applied to all sides of the model region, while no motion perpendicular to region boundaries are allowed except at the top.

Results: Figure 1 shows a typical result of the computations modeling the density changes. Density contours (0.1 g/cm^3 spacing) clearly delineate the slab and its crustal layer. In this case (10°C/km geotherm, 25 km crust, subduction rate of 5 km/m.y.) the net slab densities in the region above the basalt-eclogite phase transition are lower than their mantle surroundings (the phase change is set for the density analysis at 110 km depth). Above the 110-km depth densities in the crustal portion of the slab are lower than in the mantle outside the slab. This causes the net slab density to be less than that in the surrounding mantle. Below the basalt-eclogite phase change, net slab densities exceed those in the neighboring mantle. Net slab buoyancy remains positive until the slab has lengthened to about 275 km. Thereafter, slabs become negatively buoyant.

Initial finite element results indicate that the positively buoyant slabs will rise through the mantle at a rate of 5 to 10 km/m.y. This analysis considers only the instantaneous velocity of the slab and does not incorporate the full results of the density modeling or the dynamics of slab subductive descent.

Discussion: Qualitatively, subduction is likely to be enhanced by negatively buoyant slabs or hindered by slabs that are positively buoyant. Positive net buoyancy is found above the basalt-eclogite phase change, tending to oppose subduction. Negative net slab buoyancy for the full-length slab was found for all conditions, while neutral buoyancy was achieved for slabs at a length of about 275 km. Thus, the slab must penetrate deeply into the mantle before negative buoyancy can help drive subduction. The rate of the slab's buoyant rise through the mantle is then important in determining whether the slab may descend deeply enough to become negatively buoyant.

Preliminary results of finite element modeling indicate the slab may rise at rates between 5 and 10 km/m.y. Thus, subducting slabs will tend to rise into an underthrusting position if their subduction rate is slow. However, it may be that moderate to high rates of subduction will overwhelm the buoyant rise of a slab. This could lead to slabs being forced through the basalt-eclogite phase transition and to great enough depths to become negatively buoyant, thus possibly producing a self-sustaining subduction system.

These initial results must be considered in light of the presumption of subduction made in undertaking the analysis. Some process still must be found that would carry the slab downward despite its initial positive buoyancy. Further work will model more closely the dynamics of the subductive motion of the slab and the effects of the slab density evolution on slab buoyancy, its rate of rise through the mantle, and the continuance of subduction.

These results indicate that for all cases of assumed Venus geotherm a lithospheric slab whose subduction has been initiated will instead be forced to underthrust the overriding lithosphere if the subduction rate is slow. This could then lead to crustal thickening, melting, and volcanism, and possibly provide one model to explain the association of compressional mountain belts and blocks of high-standing tessera, with apparent flexural rises and foredeeps, and with large volumes of volcanic deposits.

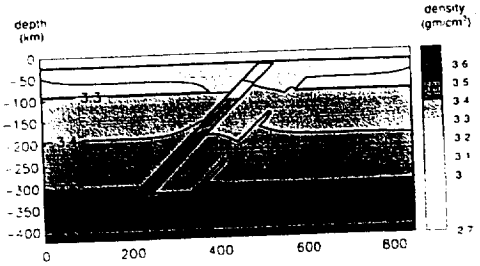

Fig. 1. Final density distribution for 10°C/km geotherm, 25 km crust, and 5 km/m.y. subduction rate. Contours have a 0.1 g/cm^3 spacing.

References: [1] Phillips R. J. and Malin M. C. (1982) in *Venus* (D. M. Hunten et al., eds.), 159–214, Univ. of Arizona, Tucson. [2] Anderson D. L. (1981) *GRL, 8*, 309–311. [3] Crumpler L. S. et al. (1986) *Geology, 14*, 1031–1034. [4] Head J. W. (1990) *Geology, 18*, 99–102. [5] Vorder Bruegge R. W. and Head J. W. (1989) *GRL, 16*, 699–702. [6] Hess P. C. and Head J. W. (1989) *Abstracts of the 28th International Geological Congress*, 2–55. [7] Minear J. W. and Toksoz M. N. (1970) *JGR, 75*, 1397–1419. [8] Turcotte D. L. and Schubert G. (1982) *Geodynamics: Applications of Continuum Physics to Geological Problems*, Wiley, New York, 450 pp. [9] Gerald C. F. (1978) *Applied Numerical Analysis, 2nd edition*, Addison-Wesley, Reading, Massachusetts.

N93-14803 P-2

EROSION VS. CONSTRUCTION: THE ORIGIN OF VENUSIAN CHANNELS. D. B. J. Bussey and J. E. Guest, University of London Observatory, University College London, London NW7 2QS, UK.

Lava channels are a common feature in the volcanic regions of the Moon, and have now been observed on Venus [1]. There has been much debate about the origin of lunar channels: Are they the result of erosional (either thermal or mechanical) or constructional processes? It is necessary to determine the criteria to distinguish between the different types of channels. The clearest evidence is that the presence of levees indicates that the channel experienced a constructional phase for a period.

Greeley [2] has proposed that Hadley Rille, on the Moon, was formed as a leveed channel and lava tube system. Evidence for this is its location along the crest of a ridge. In addition, Hadley Rille and other lunar mare sinuous rilles are discontinuous, suggesting that their origin was, in part, a lava tube that has subsequently undergone partial roof collapse. Carr [3] and Head and Wilson [4] have argued that these rilles were produced by lava erosion. For lunar highland channels, which tend to be larger than their mare counterparts, mechanical erosion of the megaregolith is a possible process.

Channels of several different types have been observed on the surface of Venus [1]. They are probably formed by more than one process. They range in size from a few kilometers to over 6800 km [1]. The relatively short ("tadpolelike") channels [5] (e.g., 24 S 347) appear similar to lunar mare sinuous rilles in morphology. They are so like certain constructional terrestrial channels (e.g., Kalaupapa, Hawaii [6]) that it appears reasonable to say that they too are constructional channels or collapsed lava tube systems.

However, the long sinuous channels referred to by Baker et al. [1] as "canali" pose a different problem in the understanding of their formation. One example of a channel of this type in the southeast region of Aphrodite Terra appears to show both erosional and constructional characteristics. This channel is represented in Fig. 1. It is approximately 700 km long with an average width of about 1 km. It drops a distance of 700 m from beginning to end, which means that the average slope is 0.06°. Its source may have been a graben situated at the northwest end of the channel. It appears to have different origins along its length.

The lack of levees near the source suggests that the channel is erosional in this region. An inferred profile is shown as AA' in Fig. 1.